Observation of visible forbidden lines of tungsten highly charged ions in LHD core plasmas and its application to ion distribution analysis

Observation of visible forbidden lines of tungsten highly charged ions in LHD core plasmas and its application to ion distribution analysis

D. Kato[1,2], H. A. Sakaue[1], I. Murakami[1,2], M. Goto[1,2], T. Oishi[1,2], K. Fujii[3], N. Nakamura[4], S. Morita[1,2], and LHD Experiment Group[1]

[1]National Institute for Fusion Science (NIFS), Toki, Gifu 509-5292, Japan

[2]SOKENDAI (The Graduate University for Advanced Studies), Toki, Gifu 509-5292, Japan

E-mail contact of main author: kato.daiji@nifs.ac.jp

Abstract. Visible emission lines of tungsten ions are useful for analysis of tungsten ion distributions at ITER because the radiation shielding of detectors is not basically necessary by using optical fibers. Here we report the result on observation of visible magnetic-dipole (M1) lines of highly-charged tungsten ions in the Large Helical Device (LHD) by tungsten pellet injection and its first application to the ion distribution analysis. Based on the measured spatial profile of an M1 line intensity of W^{27+}, tungsten ion distributions in LHD core plasmas are quantitatively analyzed using a collisional-radiative model. Strong enhancement of the M1 line intensity due to proton collisions is predicted by the present calculation. Poloidal asymmetry of the tungsten density distribution in the core plasma is inferred from the present analysis. Peak tungsten concentration at the plasma center is evaluated to be as high as 10^{-2}. Tungsten diffusion from the core plasma is observed in time variation of the deduced density profiles.

1. Introduction

Tungsten, which is used as divertor materials in ITER, will cause serious radiation loss once it accumulates in the plasma core because it is not fully ionized even in the ITER with $T_e = 15 - 20$ keV. It is, therefore, necessary for the stable operation of ITER to study the influx and edge transport of tungsten ions. Visible lines from the tungsten ions provide useful diagnostics means for ITER because the radiation shielding of detectors is not necessary by using optical fibers. However, the knowledge on visible lines of the tungsten from fusion experiments has been exclusively limited to neutral atoms and ions in low charge states.

Magnetic-dipole (M1) lines of highly-charged heavy elements in the ground states will fall in the visible range. The M1 lines of the ground states have strong intensities because of the large fractional population in plasmas. The M1 lines are isolated in emission spectra and have narrow natural widths, which are suitable for ion density and temperature measurements. Usage of such M1 lines will give a better understanding of tungsten behaviour because precise spectroscopic measurements are facilitated in the visible region.

Komatsu et al. [1] and Watanabe et al. [2] found such visible M1 lines of Cd-like W^{26+} by means of electron-beam-ion-traps (EBITs). The lines are identified as ground state ($4f^2$) fine-structure transitions [1,3]. A near-UV M1 transition of Ag-like W^{27+} in the ground state (4f) was observed in spectra measured by using a permanent magnet EBIT at Fudan University [4]. Wavelength data of visible lines from W^{8+} through W^{28+} are reported by a series of measurements using a compact EBIT (CoBIT) [5]. The first measurement of the visible M1 line emission in magnetic-confinement plasma devices was reported at the Large Helical Device (LHD) using tungsten pellet injection [6]. Precise measurements of near UV-visible forbidden lines from highly-charged ions colliding with high density hydrogen plasma particles

(electron + proton), say $10^{19\text{ - }20}$ m^{-3}, are feasible with the LHD. Therefore, the LHD enables experimental studies to identify tungsten emission lines useful for fusion plasma diagnostics and provide new spectroscopic data complementing measurements by the EBITs operating at much lower electron densities (order of 10^{16} m^{-3}). Recently, high-resolution wide-band spectral measurements in 423 – 715 nm have been performed at the LHD with a specially designed Échelle spectrometer [7]. Spatial distributions of the line intensity and polarization resolved measurements have also been performed [8].

Ionization potentials of the highly-charged ions for which the visible line emissions were observed distribute from a few hundred eV to a few keV. These ions will be abundant in edge plasmas including Scrape-Off Layer (SOL) and divertor regions of ITER, widening an application range of visible spectroscopy for tungsten ions. In the present contribution, we report the first application of the visible M1 lines to tungsten ion distribution analysis in the LHD core plasmas.

2. Experimental set-up

Tungsten was introduced into the LHD plasmas by injecting a polyethylene pellet (0.6 mm long and 0.6 mm diameter) containing a tungsten wire. Size of the tungsten wire in the polyethylene tube is 0.15 mm in diameter and 0.6 mm in length. Number of tungsten atoms in the single pellet is estimated roughly to be 6.6×10^{17}. The pellet is accelerated by pressurized He gas of 10 – 20 atm and injected with the angle of 12˚ tilted from the normal to the toroidal magnetic axis. Time-resolved (sampling times for 38 ms at every 100 ms) emission spectra are measured using a Czerny-Turner visible-UV spectrometer (grating of 1200 gr/mm and slit width of 50 μm) equipped with a CCD detector. Figure 1 shows an observation port as well as the pellet injection port. Photon emission is detected through optical fibers at 44 lines of sight along the vertical direction (Z) of a horizontally elongated poloidal cross section, as shown in Fig. 1. The poloidal cross section is asymmetric with respect to $Z = 0$ because the cross section is 6˚ tilted from the normal to the toroidal magnetic axis.

Discharges for present measurements were started with electron cyclotron heating followed by hydrogen neutral beam injection (NBI) heating. Figure 2 shows a typical time sequence of plasma parameters during the present measurements. By the pellet injection at t = 4.0 s, the central electron temperature (T_e) decreases from about 3 keV down to 2 keV in 100 ms following a stepwise enhancement of the radiation power. The line-averaged electron density (n_e) increases rapidly after the pellet injection. The line-averaged n_e keeps increasing gradually until t = 5.4 s, while the central T_e is kept almost constant at about 1 keV. From t = 5.4 s, the central T_e starts to rise, while the line-averaged n_e turns to decrease. The radiation power also decreases accompanying an increase of the stored energy.

3. Observation of visible line emissions from W^{q+} in the LHD

Tungsten spectra were measured for 320 – 356 nm and 382 – 402 nm with two different discharges (shot No. 121534 and 121541), respectively, because of a limited band width of a single measurement. T_e profiles of the two discharges with respect to the effective minor radius (see Fig. 3) are almost identical and change little during the measurements (t = 4.1 – 4.138 s), while the peak temperatures decrease from 2 keV to 1.75 keV. Wavelength calibration was done using emission lines of hydrogen and helium in the same discharges. Uncertainties in the wavelength calibration are estimated to be about 0.02 nm.

Figure 3 shows the measured spectrum in 330 – 340 nm. Emission lines indicated by red arrows in the figure are absent in a spectrum taken before the tungsten injection (drawn in the

figure by light gray color). These lines are, therefore, assigned to emission lines of the tungsten ions. Vertical profiles of line-integrated intensities of the emission lines are shown in the upper panels of the figure. The tungsten lines show intensity distributions localized inside the core plasma ($Z < 0.4$ m, i.e. $r_{\rm eff} < 0.5$ m), while other lines have broader distributions. Two lines at 333.7 nm and 335.7 nm are identified as the M1 transitions of W^{26+} ($4f^2$) $^3F_4 - {}^3F_3$ and $^3F_4 - {}^1G_4$, respectively, and one line at 337.7 nm is the M1 transition of W^{27+} (4f) $^2F_{7/2} - {}^2F_{5/2}$. 11 lines of W^{q+} (q = 20, 23−28) are identified in total for 330 – 390 nm whose wavelengths coincide with those determined by EBITs [1-5].

4. Atomic model for M1 line emission from W^{q+} in ground states

Emission line spectra of W^{q+} in hydrogen plasmas are calculated using a collisional-radiative (CR) model. In the CR model, fractional populations of excited levels $n_i^{(q)}$ of W^{q+} are obtained by solving the quasi-stationary state equation,

$$\frac{dn_i^{(q)}}{dt} = \sum_{j\neq i}\left(n_{\rm e}C_{ij}^{\rm e} + n_{\rm p}C_{ij}^{\rm p}\right)n_j^{(q)} + \sum_{j>i}A_{ij}n_j^{(q)} + n_{\rm e}\sum_j S_{ij}^{q-1\to q}n_j^{(q-1)}\,n_{q-1}/n_q$$
$$-\left[\sum_{j\neq i}\left(n_{\rm e}C_{ji}^{\rm e} + n_{\rm p}C_{ji}^{\rm p}\right) + n_{\rm e}S_i^{q\to q+1} + \sum_{j<i}A_{ji}\right]n_i^{(q)} = 0,$$

where $n_{\rm e}$ and $n_{\rm p}$ are electron and proton densities, respectively, $C_{ij}^{\rm e}$ and $C_{ij}^{\rm p}$ (de-)excitation rate coefficients by electron and proton collisions, respectively, $S_i^{q\to q+1}$ ionization rate coefficients by electron collisions, A_{ij} transition rates, and n_q fractional ion abundances of W^{q+}. The third term in the right hand side of the first equation is the population rate of the excited level by ionization excitation from $W^{(q-1)+}$. The collisional rate coefficients are calculated from cross sections assuming the Maxwellian velocity distribution of electrons and protons. The energy levels, the radiative transition rates and the electron collision cross sections are calculated using HULLAC code [10].

Emission line intensity of a transition from the upper level *j* to the lower level *i* is given by,

$$I_{ij}^{(q)} = A_{ij}n_j^{(q)}n_q n_{\rm W},$$

where $n_{\rm W}$ is tungsten density. It is assumed that cross-field ion transport in the core plasma should take place with a longer time scale than that of the ionization equilibrium (order of ms) and the transport effects on charge state distributions are insignificant. In the present model, n_q are obtained by solving the ionization equilibrium equation using electron collisional ionization and recombination rate coefficients available in databases [11,12]. The same arguments were made also in previous works by Asmussen et al [12] and Pütterich et al.[13].

Cross sections of proton collisions are calculated in a semi-classical perturbation approximation. Effective strength of Coulomb repulsive interaction between W^{q+} and a proton of an impact velocity v is represented by a characteristic parameter: $\mu = qe^2/\hbar v$, where e is the elementary charge and $\hbar$ the reduced planck constant. In cases that $\mu \gg 1$, perturbation methods are valid because the proton cannot penetrate in the vicinity of the target ion. The electric quadruple interaction is the primary part of the long-range electrostatic interaction which induces transitions in fine-structure levels of the target ion. In the semi-classical perturbation approximation (SCPT-E2), the cross section σ is expressed simply by the electric quadruple transition rate of isolate W^{q+} ions, $B(\mathrm{E2})$,

$$\sigma = \left(\frac{e}{\hbar v_{\rm i}}\right)^2 a^{-2} B({\rm E2}) f_{\rm E2}(\xi),$$

$$a = \frac{qe^2}{\mu v_{\rm i} v_{\rm f}}, \qquad \xi = \frac{qe^2}{\hbar}\left(\frac{1}{v_{\rm f}} - \frac{1}{v_{\rm i}}\right),$$

where μ is the reduced mass of a proton and a target ion, and $v_{\rm i,f}$ are velocities of incident and scattered protons, respectively. $f_{\rm E2}(\xi)$ is a function given by assuming hyperbolic orbit for the proton in the Coulomb filed centred at the nucleus of W^{q+} [14]. The electric quadruple transition rates are calculated using the HULLAC code. In order to evaluate accuracy of the present method, excitation rate coefficients in Fe^{13+} 3p doublet state are calculated and compared with recommended data [15]. SCPT-E2 cross sections give rate coefficients which coincide with the recommended values at low temperatures but overshoot at high temperatures. About factor of 3 larger at the peak temperature of the equilibrium ion abundance. It is noted that simple mass-scaling of electron distorted-wave cross sections underestimates the rate coefficients by many orders of magnitudes.

Fractional populations of excited levels are calculated by the CR model for W^{27+}. As shown in Fig. 4, the fractional population distribution is drastically changed by proton collision effects. The proton collision facilitates redistribution in populations of quasi-degenerate excited levels, which causes depopulation of meta-stable levels in the sub-valence excited $4d^9 4f^2$ configuration. Fractional populations of the ground state are, therefore, increased via 4f - 4d allowed transitions from the excited configuration resulting in an enhancement of the ground-state M1 line intensity. It is noted that the 4f - 4d EUV emission line intensities are also increased.

5. W density analysis base on an M1 line intensity profile of W^{27+} in the LHD

Figure 5 shows line-integrated intensities of the W^{27+} M1 line (337.7 nm) at five successive periods in one measurement depicting variation of its vertical profiles in time. Theoretical vertical profiles are calculated by the CR model using $T_{\rm e}$ and $n_{\rm e}$ distributions with respect to the effective minor radius measured by Thomson scattering. It is assumed that values of $T_{\rm e}$ and $n_{\rm e}$ on each effective minor radius are constant. The measured profiles are fitted well with the theoretical profiles using tungsten density distributions shown in Fig. 6. However, the measured vertical profiles show systematically larger intensities than the theoretical profiles in $Z < 0$. Poloidally symmetric tungsten density distribution is assumed in the present calculation, i.e. $n_{\rm W}(r_{\rm eff}) = n_{\rm W}(0)\exp\left[-a \times r_{\rm eff}^2\right]$. Small but significant deviations from the measurements can be ascribed to poloidal asymmetry in the density distribution.

In Figure 6, radial profiles of $n_q n_{\rm W}$ for W^{q+} and $n_{\rm W}$ which are deduced by fitting to the vertical profiles of Fig. 5 are shown. The $n_{\rm W}(r_{\rm eff})$ distribution at 4.1 s is uniform throughout the core plasma giving $n_{\rm W}(0)/n_{\rm e}(0) \sim 1/3 \times 10^{-2}$. The density in the core plasma is initially increased until t = 4.3 s accompanying a temperature drop and a density rise. The peak tungsten density at the plasma center is as high as $n_{\rm W}(0)/n_{\rm e}(0) \sim 10^{-2}$. Using available radiation power rates of tungsten [16], radiation power densities due to tungsten line emissions at the plasma center are roughly estimated to be 1.8 – 5 MW/m^3, while the total radiation power is about 3.5 MW. The apparent decrease in $n_{\rm W}$ for t = 5.0 – 5.6 s indicates diffusion of the tungsten ions after confinement in the plasma center. It is noted that a time scale of the diffusion is apparently much longer than that of the ionization equilibrium for W^{27+} ions.

The deduced tungsten densities will be increased by a factor of two by neglecting the proton collision because the line-integrated intensities reduce almost by half. The deduced density

values are sensitive to accuracy of the proton rate coefficients. It is problematic to quantify uncertainty in the present analysis because available atomic data on the proton rate coefficients for W^{q+} are extremely limited.

6. Summary

The ground state M1 lines of W^{q+} are useful for diagnostics of W^{q+} ions in ITER. 11 lines from W^{q+} (q = 20, 23−28) in the LHD are observed at 330 – 390 nm whose wavelengths coincide with those determined by EBITs [1-5].

Proton collision effects in the M1 line intensities are investigated using proton collision cross sections calculated in a semi-classical perturbation theory. In high-temperature plasmas, the proton collision facilitates population redistribution in quasi-degenerate levels of fine-structures reducing meta-stable excited state population, which results in enhancement of the ground state population. As a result, the M1 line intensities of ions in the ground states are increased by the proton collisions. By including the proton collision, the M1 line intensity of the ground state W^{27+} is increased to almost double.

Vertical profiles of the M1 line intensity of the ground state W^{27+} are compared with calculations by the CR model. The vertical profiles cannot be reconciled with theoretical profiles calculated assuming poloidally symmetric tungsten density distributions indicating poloidal asymmetry in the tungsten density distribution.

The peak tungsten density at the plasma center deduced from the measured M1 line intensity becomes very high giving $n_{\mathrm{W}}(0)/n_{\mathrm{e}}(0) \sim 10^{-2}$. The density in the core plasma decreases with time due to cross-field diffusion of the tungsten ions after confinement in the plasma center. The diffusion apparently takes place with a longer time scale than that of the ionization equilibrium indicating decoupling of the ion transport from the charge-changing (ionization/recombination) processes of W^{q+} ions in core plasmas.

Acknowledgements

This work was performed under the auspices of the NIFS Collaboration Research program (NIFS13KLPF032, NIFS16KLPF052) and the JSPS-NRF-NSFC A3 Foresight Program in the field of Plasma Physics (NSFC: No.11261140328, NRF: No.2012K2A2A6000443). DK is grateful to financial support of KAKENHI (15H04235).

[1] KOMATSU, A., et al., Phys. Scr. **T144** (2011) 014012.

[2] WATANABE, H., et al., Can. J. Phys. **90** (2012) 197.

[3] DING, X.-B., et al., J. Phys. B: At. Mol. Opt. Phys. **44** (2011) 145004.

[4] FEI, Z., et al., Phys. Rev. A **86** (2012) 062501.

[5] KOMATSU, A., et al., Plasma and Fusion Res.: Rapid Commun. **7** (2012) 1201158.

[6] KATO, D., et al., Phys. Scr. **T156** (2013) 014081.

[7] SHINOHARA, M., et al., Phys. Scr. **90** (2015) 125402.

[8] FUJII, K., et al., Phys. Scr. **90** (2015) 125403.

[9] QUI, M., et al., J. Phys. B: At. Mol. Opt. Phys. **47** (2014) 175002.

[10] BAR-SHALOM, A., et al., J. Quant. Spectr. Radiant. Trans. **71** (2001) 169.

[11] The Atomic Data and Analysis Structure (ADAS), http://open.adas.ac.uk/.

[12] ASMUSSEN, K., et al., Nucl. Fusion **38** (1998) 967.

[13] PÜTTERICH, T., et al., Plasma Phys. Control. Fusion **50** (2008) 085016.

[14] ALDER, K. et al., Rev. Mod. Phys. **28** (1956) 432.

[15] SKIBELEV, I., et al., NIFS-DATA-**95** (Jan. 2006).

[16] MURAKAMI, I., et al., Nucl. Fusion **55** (2015) 093016.

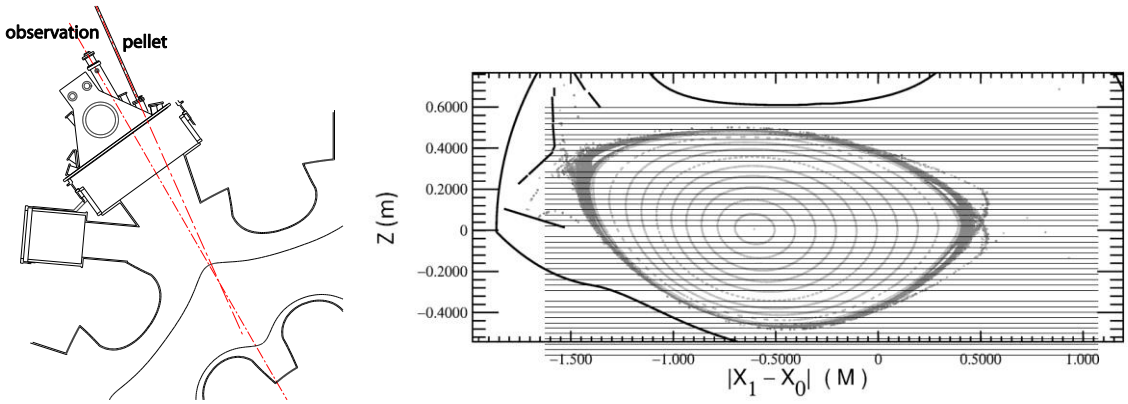

FIG. 1. Left) A top view of the observation and pellet injection ports. Right) Horizontally elongated poloidal cross section and lines of sight. Viewing point is on the right-hand side.

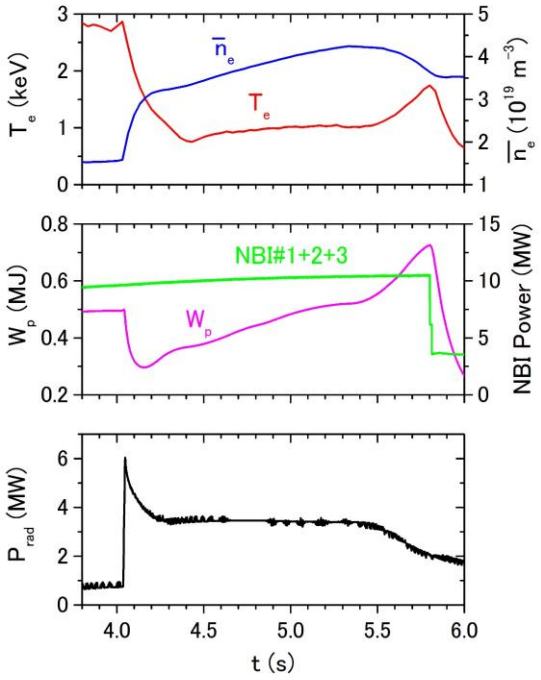

FIG. 2. Time traces of (Upper) central electron temperature and line-averaged electron density, (Middle) stored energy (W_p) and NBI port-through power and (Bottom) total radiation power. A tungsten pellet is injected at 4.0 s.

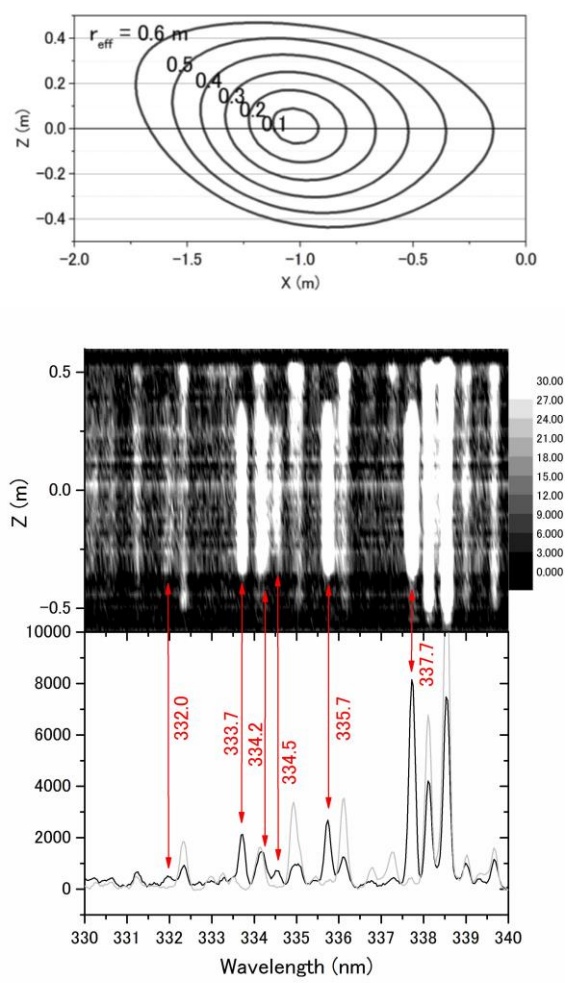

FIG. 3. Upper) Contour plot of effective minor radius r_{eff} on the poloidal cross section.

Lower) Line emission spectra in 330 – 340 nm measured at the LHD (shot No. 121534). Upper panel shows vertical profiles of line-integrated intensities. Solid indicates the spectrum measured after tungsten injection (t = 4.1 – 4.138 s), and light gray before the tungsten injection. Red arrows indicate emission lines assigned to tungsten highly charged ions. Numbers are the central wavelengths in nm.

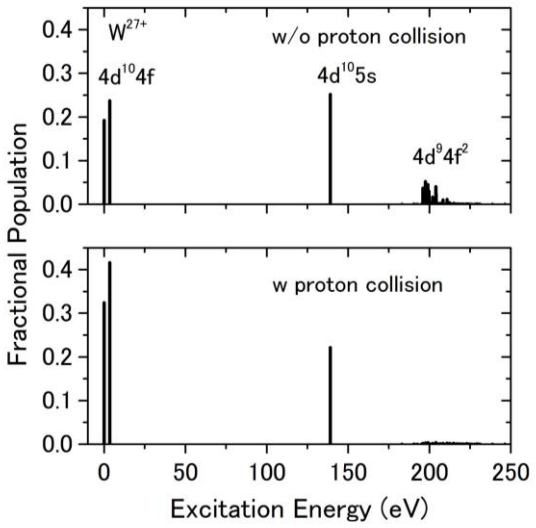

FIG. 4. Fractional populations of W^{27+} levels without proton collision (upper) and with proton collision (lower). $n_e = n_p = 10^{13}$ cm^{-3} and $T_e = T_p = 1$ keV are assumed.

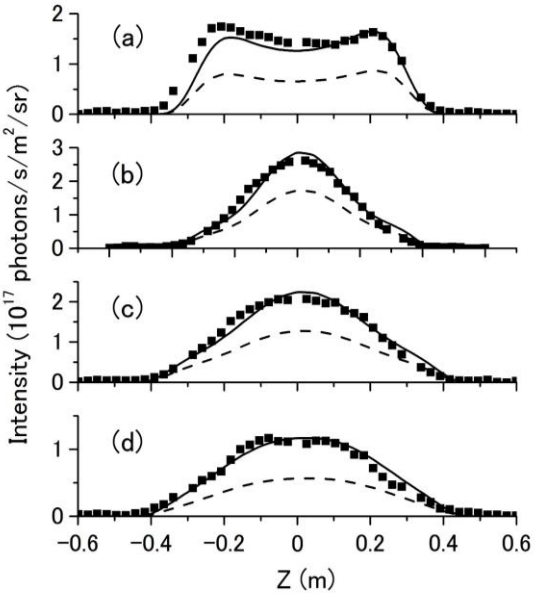

FIG. 5. Vertical distributions of line-integrated intensities of W^{27+} M1 line at (a) t = 4.1, (b) 4.3, (c) 5.0 and (d) 5.6 s. Tungsten pellet is injected at 4.0 s. Solid squares indicate measurement and solid curves calculations, respectively. Dashed lines are the calculation neglecting proton collision effects.

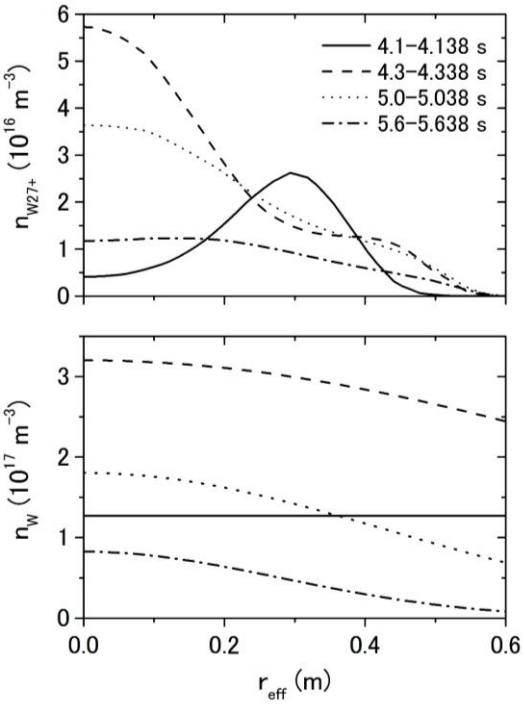

FIG. 6. Radial profile of $n_q n_W$ for W^{27+} ions (Upper) and n_W (Lower), respectively, which are deduced by fitting to the vertical profiles of FIG. 5. Peak temperatures at the plasma center are 2.0, 1.0, 1.0, and 1.2 keV at 4.1, 4.3, 5.0 and 5.6 s, respectively.